Cement and Concrete Research 113 (2018) 13–26

Contents lists available at ScienceDirect

Cement and Concrete Research

journal homepage: www.elsevier.com/locate/cemconres

May reversible water uptake/release by hydrates explain the thermal expansion of cement paste? — Arguments from an inverse multiscale analysis

Hui Wang[a,b], Christian Hellmich[a], Yong Yuan[b], Herbert Mang[a,b], Bernhard Pichler[a,*]

[a] Institute for Mechanics of Materials and Structures, TU Wien — Vienna University of Technology, Karlsplatz 13/202, Vienna A-1040, Austria
[b] College of Civil Engineering, Tongji University, Shanghai, China

ARTICLE INFO

Keywords:
Coefficient of thermal expansion
Poromechanics
Poroelasticity
Multiscale analysis
Partial saturation

ABSTRACT

Quasi-instantaneous thermal expansion of cement pastes is governed by the relative humidity (*RH*) within their air-filled pores and by the decrease/increase of this internal *RH* resulting from a temperature decrease/increase. The latter effect is traced back to quasi-instantaneous water uptake/release by cement hydrates, using micro-poromechanics and a three-scale representation of mature cement pastes. Partially saturated gel and capillary pores are considered to be connected and spherical, with radii following exponential distributions. The Mori-Tanaka scheme provides the scale transition from effective pore pressures to eigenstrains at the cement paste level. This modeling approach, together with considering mass conservation of water, allows for downscaling macroscopic thermal expansion coefficients, so as to identify the molecular water uptake/release characteristics of the hydrates. The latter characteristics are mixture-independent, as shown by their use for predicting the thermal expansion coefficients of different mature cement pastes, with *w/c*-ratios ranging from 0.50 to 0.70.

1. Introduction

External heating/cooling of a millimeter-to-decimeter-sized sample of partially saturated (drained) cement paste actives two transport processes. Heat transport provides the transition between two different isothermal states [1-3]. This takes typically from minutes to hours, depending on the size of the specimen and on the magnitude of the temperature change, ΔT. The increase/decrease of temperature goes hand in hand with both thermal expansion/contraction of the cement paste sample *and* an increase/decrease of its internal relative humidity. The latter change activates a moisture transport process between the open porosity of the specimen and the ambient air. This takes typically from days to weeks. The corresponding deformation partly recovers the thermal expansion/contraction [1,2,4]. In saturated (or close to saturated) conditions, delayed deformations under constant temperature have been attributed to macroscopic water transport caused by overpressure of water expanding more than the solid skeleton, see Ref. [5].

The coefficient of thermal expansion of mature cement paste ranges from $8 \cdot 10^{-6}\,\mathrm{K}^{-1}$ to $22 \cdot 10^{-6}\,\mathrm{K}^{-1}$ and appears as an asymmetrical bell-shaped function of relative humidity which prevails in the air-filled pores just *before* the applied temperature change, see Refs. [6-10] and Fig. 1. Knowledge of such thermal expansion coefficients is important for practical applications in concrete construction, see, e.g. Ref. [11]. In this context, it is noteworthy that concrete aggregates have typically smaller thermal expansion coefficients, ranging between $4 \cdot 10^{-6}\,\mathrm{K}^{-1}$ and $12 \cdot 10^{-6}\,\mathrm{K}^{-1}$, depending on the mineral composition [9,12,13]. Therefore, subjecting concrete to a temperature change, yields a mismatch of thermal eigenstrains. This results in thermal (micro-)stresses, which may even cause microcracking [14-16], reducing the durability of concrete structures.

Quasi-instantaneous expansion due to the temperature increase ΔT goes hand in hand with an *increase* of the internal relative humidity ΔRH, see, e.g. measurements documented in Refs.[2,10,17-19]. These experimental data suggest that the ratio $\Delta RH/\Delta T$, referred to as the hygrothermic coefficient [3], is a nonlinear function of the internal relative humidity which prevails in the air-filled pores just *before* the temperature change, see Fig. 2. In addition, the hygrothermic coefficient is considered to depend on the initial water-to-cement mass ratio [3,19], but the underlying physical processes are still not fully understood.

The ongoing scientific discussion regarding the origin of hygrothermic coefficients mainly concerns the redistribution of liquid water. In this context, Bažant [2] attributed hygrothermic coefficients to water migration from gel pores to capillary pores, considering that increasing

* Corresponding author.
E-mail address: Bernhard.Pichler@tuwien.ac.at (B. Pichler).

https://doi.org/10.1016/j.cemconres.2018.05.008
Received 7 July 2017; Received in revised form 27 March 2018; Accepted 8 May 2018
Available online 18 July 2018

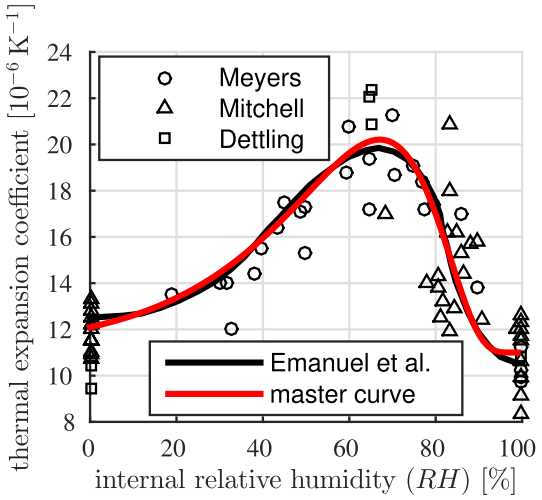

Fig. 1. Relation between the coefficient of thermal expansion and the internal relative humidity which prevails in the air-filled pores, just *before* the temperature change: experimental data from Meyers [6], Mitchell [7], and Dettling [8], measured on mature cement pastes with initial water-to-cement mass ratios $w/c \in [0.12; 0.40]$; the curve described by Emanuel et al. [9]; and the "master curve" given in Eq. (3).

temperature causes a chemical potential difference between the gel and the capillary water. Grasley et al. [10] and Radjy et al. [19] estimated temperature-induced changes of relative humidity *RH*. For that, they used Kelvin's equation, considered that the surface tension at liquid-gas interfaces decreases with increasing temperature according to measurements [20], and treated the radius of the corresponding meniscus between pore water and air as a constant. The correspondingly estimated increase of relative humidity underestimates the measured hygrothermic coefficients. Therefore, Grasley and Lange proposed water expansion in ink-bottle pores to be responsible for the aforementioned measured values of hygrothermic coefficients [10]. This indicates that the radius of the meniscus between the pore water and the air increases with increasing temperature. Wyrzykowski and Lura [21] obtained hygrothermic coefficients by means of water activity and sorption measurements. The two independent methods associated with the aforementioned measurements delivered consistent results. Using a model linking capillary pressure to elastic deformation [22-24], Wyrzykowski and Lura related the measured early-age evolution of the hygrothermic coefficients to the measured coefficients of thermal expansion. They did so for samples aged between 1 and 7 days [21], when the measured relative humidity decreased from full saturation to values, ranging between 85% and 94%. Still, modeling of hygrothermic coefficients of mature cement pastes in the regime of intermediate relative humidities from 25% to 85% remains an open research question.

Existing models for thermal expansion of cement paste are of hygrothermoporoelastic and macroscopic nature. They typically consider two contributions: (i) thermal expansion of the solid skeleton, α_{cp}^{sol}, and (ii) hygrothermic expansion resulting from pore pressure changes [2,10,21,25], α_{cp}^{hyg}:

$$\alpha_{cp}^{mod} = \alpha_{cp}^{sol} + \alpha_{cp}^{hyg}. \tag{1}$$

As regards the latter, the Kelvin-Laplace equation is used to quantify capillary pressure from knowledge on temperature and relative humidity. Increasing temperature and the associated increase of internal relative humidity result in a decrease of capillary pressure Δp_c and an increase of the saturation ratio ΔS_r. The resulting hygrothermic expansion $\Delta\varepsilon_{hygro}$ is typically quantified as [10,21,24]

$$\Delta\varepsilon_{hygro} = \frac{\Delta p_c\, S_r + p_c\, \Delta S_r}{3}\left(\frac{1}{k_{\mathrm{hom}}} - \frac{1}{k_s}\right), \tag{2}$$

where k_{hom} and k_s, respectively, are the bulk moduli of the porous material and of the solid skeleton. Eq. (2) is theoretically rigorous for liquid saturation, i.e. for $S_r = 100\%$, see Refs. [21,24], and it is of approximate nature in case of partial saturation [24,26]. While Eq. (2) could be shown to be reliable for saturation degrees $S_r \geq 80\%$, it underestimates the hygrothermic expansion at smaller saturation degrees [21,24].

In the present paper, hygrothermic coefficients and thermal expansion of mature cement pastes are explained by quasi-instantaneous uptake or release of water by the hydrates. This is an effect for which no physical measurements were available at the time of submitting the present manuscript. However, such measurements were reported shortly thereafter [27]. In the present context of modeling, the hydrates are, in the sense of a reductionist approach, not subdivided explicitly into different hydration products, such as calcium-silicate-hydrates (C-S-H), portlandite, and ettringite. Still, it is noteworthy that water (H) in the C-S-H can be considered to be at least partly mobile [28,29], while the water chemically bound in crystalline products, such as portlandite and ettringite, cannot be considered as at least partially mobile.

Methods of microporomechanics [26,60] in combinations with the mass conservation law are used to identify the quasi-instantaneous uptake or release of water by hydrates, with focus on mature cement pastes and on the central regime of relative humidities ranging from 25% to 85%. To this end, unhydrated clinker grains, hydrates, capillary pores, and gel pores are introduced as elementary constituents in a three-scale representation of mature cement pastes. The pores are considered to be well connected and spherical. They are either filled by water or by air, following the Kelvin-Laplace equation. Thin layers of adsorbed water are taken into account at solid surfaces, including the surfaces of "air-filled" pores [30]. The size distributions of gel and capillary pores are modeled by exponential distributions, following Huang et al. [31]. These distributions are identified such that the model-predicted adsorption isotherms agree as well as possible with

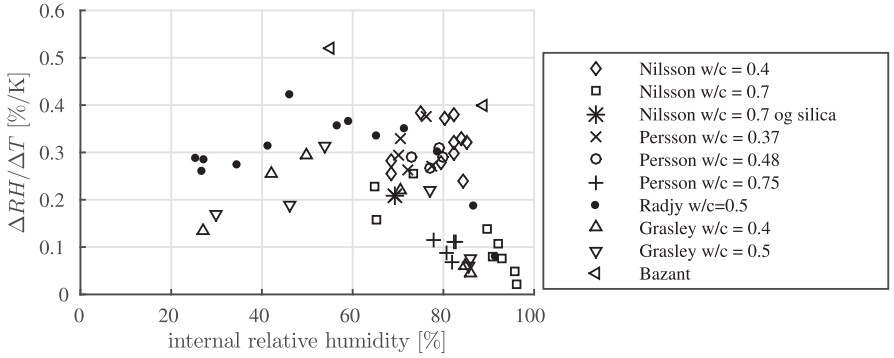

Fig. 2. Hygrothermic coefficient of cement paste as a function of the internal relative humidity, prevailing just *before* the temperature change: test results from Nilsson [17], Persson [18], Radjy et al. [19], Grasley et al. [10], and Bažant [2].

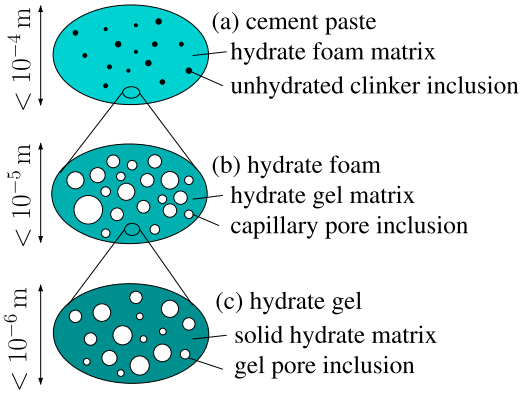

Fig. 3. Micromechanical representation ("material organogram") of mature cement pastes (a) cement pastes consist of spherical unhydrated clinker grains, embedded in a hydrate foam matrix; (b) the hydrate foam consists of spherical capillary pores, embedded in a hydrate gel matrix; (c) the hydrate gel consists of spherical gel pores, embedded in a solid hydrate matrix; two dimensional sketches of three dimensional representative volume elements.

corresponding Brunauer-Xi-type adsorption isotherms [32,33]. In the context of fluid-solid interactions, the solid skeleton of cement pastes is assumed to be loaded by effective pore pressures. The latter combine the actions of fluid pressure and surface tension prevailing at solid-fluid interfaces [26,34,35]. Effective pore pressure changes are quantified from temperature changes and from the corresponding changes of the internal relative humidity. The required scale transitions to macroscopic thermal eigenstrains of cement pastes are established by the Mori-Tanaka scheme [36,37,59]. The resulting analytical multiscale model provides the desired link between the macroscopic thermal expansion of cement pastes and hygrothermic coefficients. The water uptake/release by hydration products is finally identified, in the context of inverse multiscale analysis, starting from the hygrothermic coefficients and based on the mass conservation of solid and liquid water inside a tested specimen. This is motivated by the fact that temperature changes typically take place in time intervals which are significantly shorter than the ones required for a significant exchange of water between the cement paste samples and their ambient environment. The corresponding mass balance includes water which is bound inside solid hydrates, bulk pore water, and water adsorbed to solid surfaces.

In order to identify water uptake/release coefficients and to show that they are a material property of hydrates, independent of the composition of cement pastes, the paper is structured as follows. Measured thermal expansion coefficients of cement pastes with initial water-to-cement mass ratio $w/c = 0.40$ are downscaled in order to identify the temperature-induced water uptake/release by hydrates as a function of the relative humidity and the temperature change, see Section 2. Considering the identified water uptake/release characteristics to be a mixture-independent material property of hydrates, the multiscale hygrothermoporomechanics model is used to *predict* w/c-dependent hygrothermic coefficients and macroscopic thermal expansion coefficients of cement pastes with w/c values ranging from 0.50 to 0.70, see Section 3. A discussion, see Section 4, is followed by concluding remarks, see Section 5.

2. Top-down identification of the water uptake/release by hydration products as a function of the internal relative humidity and the temperature change

2.1. Thermal expansion of mature cement paste as a function of the internal relative humidity

Meyers [6], Mitchell [7], and Dettling [8] measured the thermal expansion of mature cement pastes (at material ages up to six months) as a function of the relative humidity, see Fig. 1. Independent of the initial water-to-cement mass ratio, $w/c \in [0.12; 0.40]$, the smallest thermal expansion develops at full saturation ($RH = 100\%$). The maximum thermal expansion is virtually twice as large and develops at $RH \approx 65\%$, and the thermal expansion at the fully dried state ($RH = 0\%$) is only slightly larger than the one at full saturation. The following regression function reproduces the experimental data satisfactorily

$$\alpha_{cp}^{\exp} = \left\{ \frac{0.3188}{1 - RH} \exp\left[-\left(\frac{\ln(1 - RH) + 0.821}{0.7605} \right)^2 \right] + 1 \right\} \times 11{\cdot}10^{-6}\ \mathrm{K}^{-1}. \tag{3}$$

It is very similar to the non-analytic fitting function used by Emanuel and Hulsey [9], see Fig. 1.

2.2. Hierarchical organization of mature cement pastes, elastic constants, and volume fractions

Cement pastes are (micro-)heterogeneous materials, consisting of unhydrated cement clinker grains, hydration products, called hydrates, and water- or air-filled gel and capillary pores, with typical lengths ranging from a few nanometers to several tens of micrometers. The hierarchical organization of cement pastes is modeled by means of three matrix-inclusion composites, introduced at different scales of observation: (i) cement paste consists of a hydrate foam matrix, hosting spherical unhydrated clinker inclusions (Fig. 3a); (ii) the hydrate foam consists of a hydrate gel matrix surrounding the spherical capillary pores (Fig. 3b); and (iii) the hydrate gel consists of a solid hydrate matrix with embedded spherical gel pores, (Fig. 3c). This is a simplified version of the hierarchical representation introduced in [39], which is admissible in the case of mature cement pastes where the specific morphology of the gel-porous hydrates does not play an important role [38]. This allows for consideration of a continuous solid hydrate matrix (Fig. 3c).

Hydrates and clinker are considered to be isotropic. Their elastic stiffness tensors are expressed in terms of their bulk moduli, k, and shear moduli, μ:

$$\mathbb{C}_k = 3k_k \mathbb{I}_{vol} + 2\mu_k \mathbb{I}_{dev}, \quad k \in \{clin, hyd\}, \tag{4}$$

with [39,40]

$$\begin{aligned} k_{clin} &= 116.7\ \mathrm{GPa}, \quad \mu_{clin} = 53.8\ \mathrm{GPa}, \\ k_{hyd} &= 31.8\ \mathrm{GPa}, \quad \mu_{hyd} = 19.1\ \mathrm{GPa}. \end{aligned} \tag{5}$$

In Eq. (4), $\mathbb{I}_{dev}$ stands for the deviatoric part of the fourth-order unity tensor, defined as $\mathbb{I}_{dev} = \mathbb{I} - \mathbb{I}_{vol}$, where $\mathbb{I}$ is the symmetric fourth-order unity tensor with components $I_{ijrs} = 1/2\ (\delta_{ir}\delta_{js} + \delta_{is}\delta_{jr})$, and $\mathbb{I}_{vol} = \frac{1}{3}(\boldsymbol{1} \otimes \boldsymbol{1})$ stands for the volumetric part of the fourth-order unity tensor, where $\boldsymbol{1}$ denotes the second-order unity tensor with the Kronecker delta δ_{ij} as its components, i.e. $\delta_{ij} = 1$ for $i = j$, and $\delta_{ij} = 0$ otherwise. Pores, in turn, are characterized by a vanishing solid stiffness: $\mathbb{C}_{cpor} = \mathbb{C}_{gpor} = 0$.

The volume fractions of the cement paste constituents are functions of the initial water-to-cement mass ratio, w/c, and of the hydration degree ξ [41-44]. They are quantified based on Powers' 1946/1957 hydration model [41,42], see also Refs.[43,44] for detailed descriptions. At the cement paste scale, the volume fractions of the hydrate foam matrix and of the unhydrated clinker grains read as [39]:

$$f_{hf}^{cp} = \frac{w/c + 0.32\,\xi}{w/c + 0.32}, \quad f_{clin}^{cp} = \frac{0.32\,(1 - \xi)}{w/c + 0.32}. \tag{6}$$

At the hydrate foam scale, the volume fractions of the hydrate gel matrix and of the capillary pores read as [39]:

$$f_{gel}^{hf} = \frac{0.68\,\xi}{w/c + 0.32\,\xi}, \quad f_{cpor}^{hf} = \frac{w/c - 0.36\,\xi}{w/c + 0.32\,\xi}. \tag{7}$$

At the hydrate gel scale, the volume fractions of the solid hydrate

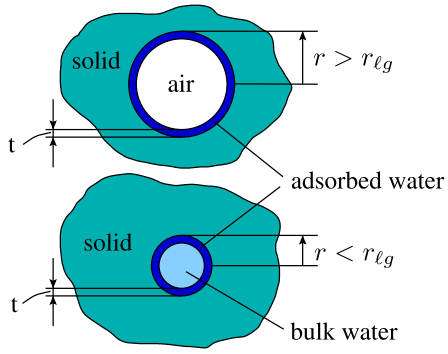

Fig. 4. Sketch of the pores coated by absorbed water at their surfaces, and filled either with air or pore water; two dimensional sketches of three dimensional configurations.

matrix and of the gel pores read as [40]:

$$f_{hyd}^{gel} = 0.72, \quad f_{gpor}^{gel} = 0.28. \tag{8}$$

2.3. Effective pore pressures acting on the solid skeleton

Pores in cement paste are either filled by pore water or occupied by air, with thin layers of adsorbed water covering the pore surfaces, see Fig. 4. The thickness of these layers, t, increases with increasing relative humidity, as quantified by [30]:

$$t = 0.385 \text{ nm} - \ln[-\ln(RH)] \cdot 0.189 \text{ nm}. \tag{9}$$

The thickness of these layers also appears in the Kelvin-Cohan equation for the radius $r_{\ell g}$ [45], discriminating between water-filled and air-filled pores,

$$r_{\ell g} = -\frac{2\,\gamma^{\ell g}\,\nu_m\cos\theta}{\ln(RH)RT} + t. \tag{10}$$

Pores with radii $r \le r_{\ell g}$ are filled with water, while pores with $r > r_{\ell g}$ are filled with air, see Fig. 4. In Eq. (10), $R = 8.31446\,\text{J mol}^{-1}\,\text{K}^{-1}$, T, and $\gamma^{\ell g}$ denote the universal gas constant, the absolute temperature, and the temperature-dependent surface tension of interfaces between liquid and gas [20], respectively; ν_m is the molar volume of water, which is equal to the molar mass of water $M_{H_2O} = 18.016\,\text{g mol}^{-1}$, divided by its temperature-dependent mass density [46], see Table 1; θ is the contact angle between the liquid and the solid, which is so small that it is usually set equal to zero for cement-based materials, i.e. pore water is considered to be an almost perfectly wetting liquid [22,47,48]. Consideration of the temperature-dependent mass density of bulk water (Table 1) is the way thermal expansion of bulk pore water is accounted for in the present contribution, see also Section 4.3.

The solid skeleton of cement pastes is subjected to effective pore pressures p, combining the effects of fluid pressure and surface tension [26,34,35]. Because of the latter, the effective pressures are functions of the pore radius r [34]

Table 1
Temperature-dependent surface tension [20], mass density [46], and molar volume of water.

Temperature [K]	Surface tension [N m^{-1}]	Mass density [kg m^{-3}]	Molar volume [m^3 mol^{-1}]
293.15	0.072750	998.2067	$18.048\cdot10^{-6}$
294.15	0.072598	997.9950	$18.052\cdot10^{-6}$

$$p(r) = \begin{cases} p_\ell - \dfrac{2\,\gamma^{s\ell}}{r-t} & \cdots \quad r \le r_{\ell g}, \\ p_g - \dfrac{2\,\gamma^{sg}}{r-t} & \cdots \quad r > r_{\ell g}, \end{cases} \tag{11}$$

where $\gamma^{s\ell}$ and γ^{sg} denote the surface tension at the solid-liquid and the solid-gas interfaces, respectively. The difference between the gas pressure p_g and the liquid pressure p_ℓ is defined as the capillary pressure p_c [35], i.e.

$$p_c = p_g - p_\ell, \tag{12}$$

which follows from the Kelvin-Laplace equation, reading as

$$p_c = -\ln(RH)\frac{RT}{\nu_m}. \tag{13}$$

Equilibrium at the 2D liquid-gas interfaces, also called “menisci”, entails that capillary pressure is proportional to the mean curvature of the menisci [34]

$$p_c = \gamma^{\ell g}\,|\text{tr}\mathbf{b}|, \tag{14}$$

where $\mathbf{b}$ denotes the curvature tensor of the menisci, and “tr” stands for “trace”. In the present context of spherical pores, the menisci are spherical. Accordingly, $|\text{tr}\mathbf{b}|$ is equal to $2/r_{\ell g}$ in case of a perfectly wetting fluid, and equal to $2\cos\theta/r_{\ell g}$ otherwise [49]. Applying the Cohan-extension to the latter expression yields

$$|\text{tr}\mathbf{b}| = \frac{2\cos\theta}{r_{\ell g} - t}. \tag{15}$$

Insertion of Eq. (15) into Eq. (14), and of the resulting expression for p_c into Eq. (13), yields, after re-arrangement of terms, the expression for $r_{\ell g}$ according to Eq. (10). Thus, the present developments consider that the size of the menisci is a nonlinear function of the relative humidity and the temperature, as described by the Kelvin-Laplace equation. As the pores of the cement pastes are assumed to be well-connected, the gas pressure p_g is set equal to the atmospheric pressure. Moreover, in the sense of a reference pressure, the latter is set equal to zero. Thus, Eq. (12) results in

$$p_g \equiv 0, \quad p_\ell = -p_c. \tag{16}$$

The surface tensions in Eqs. (10) and (11) occur in Young's equation, describing the thermodynamic equilibrium of a solid-liquid-gas system:

$$\gamma^{\ell g}\cos\theta = \gamma^{sg} - \gamma^{s\ell}. \tag{17}$$

Out of the four quantities in Eq. (17), only the surface tension between the liquid and the gas $\gamma^{\ell g}$ and the contact angle θ are directly measurable [20]. As a remedy, Berthelot's state equation [50-52], see Appendix A, is used as a supplementary element for quantification of γ^{sg} and $\gamma^{s\ell}$:

$$\gamma^{s\ell} = \gamma^{\ell g} + \gamma^{sg} - 2\sqrt{\gamma^{\ell g}\,\gamma^{sg}}. \tag{18}$$

Considering an almost perfectly wetting fluid, $\theta \approx 0$, resulting in $\cos\theta \approx 1$, and combining Eqs. (17) and (18), gives

$$\gamma^{sg} = \gamma^{\ell g}, \quad \gamma^{s\ell} = 0. \tag{19}$$

Consideration of Eqs. (13), (16), and (19) in Eq. (11) simplifies the expression for the effective pressures as follows:

$$p(r) = \begin{cases} \ln(RH)\dfrac{RT}{\nu_m} & \cdots \quad r \le r_{\ell g}, \\ -\dfrac{2\,\gamma^{\ell g}}{r-t} & \cdots \quad r > r_{\ell g}. \end{cases} \tag{20}$$

Notably, both the molar volume of water, ν_m, and the surface tension $\gamma^{\ell g}$ are temperature-dependent, see Table 1, and the thickness of the adsorbed water layer, t, is a function of the internal relative humidity, see Eq. (9).

For upscaling of these effective pressures to the material scale of

cement pastes, *average* effective pore pressure of gel and capillary pores, p_{gpor} and p_{cpor}, are relevant [34,35]. Their quantification requires a mathematical description of the pore size distributions of the gel and the capillary pores. Following Refs.[31,53], exponential distributions are introduced, i.e. the pore size probability distribution functions read as

$$\phi_k^{pdf}(r) = \frac{1}{R_k}\exp\left(-\frac{r}{R_k}\right), \quad k \in [gpor;\ cpor], \tag{21}$$

with R_{gpro} and R_{cpor} as the characteristic radii of the gel and the capillary pores, respectively, and with $\phi_{gpor}^{pdf}\mathrm{d}r$ and $\phi_{cpor}^{pdf}\mathrm{d}r$ representing the portions of the gel and capillary porosity which are associated to pores with radii ranging from r to $(r + dr)$. This allows for averaging the effective pressures (Eq. (20)) individually over the respective pore size distributions of the gel and the capillary pores as

$$p_k = \frac{1}{R_k}\int_0^\infty p(r)\exp\left(-\frac{r}{R_k}\right)\mathrm{d}r, \quad k \in [gpor;\ cpor]. \tag{22}$$

Notably, R_{gpor} and R_{cpor} represent the characteristic radii of the gel and the capillary pores, respectively.

2.4. Identification of characteristic pore radii, R_{gpor} and R_{cpor}, from adsorption porosimetry

Adsorption porosimetry [54-56] starts from a dried reference state and quantifies the mass of liquid water m_{H_2O} entering the specimen during a step-by-step increase of the relative humidity. Because complete drying is difficult to achieve [54], a small value of relative humidity, (herein: $RH = 1\%$), is associated with the dried reference state. Therefore, the modeled saturation ratio $S_r^{mod} \in [0; 1]$ follows as:

$$S_r^{mod} = \frac{m_{H_2O}(RH) - m_{H_2O}(RH = 1\%)}{m_{H_2O}(RH = 100\%) - m_{H_2O}(RH = 1\%)}. \tag{23}$$

In order to link the water mass m_{H_2O} in Eq. (23) to the pore size distributions (Eq. (21)), the total pore space (i.e. the sum of gel and capillary pores) is subdivided into a water-filled part (bulk water and adsorbed water) and an air-filled part, discriminated based on r_{lg}, see Eq. (10). The corresponding volume fractions add up to one: $f_{H_2O}^{por} + f_{air}^{por} = 1$, such that $f_{H_2O}^{por} = 1 - f_{air}^{por}$. These volume fractions provide access to the water mass inside the pores as

$$m_{H_2O} = \rho_{H_2O}\, V_{por}\, f_{H_2O}^{por} = \rho_{H_2O}\, V_{por}\,(1 - f_{air}^{por}), \tag{24}$$

where V_{por} is the total pore volume and ρ_{H_2O} is the temperature-dependent water mass density [46]. The volume fraction of air is obtained by integration over the "air-filled" pores as

$$f_{air}^{por} = \int_{r_{lg}(T,RH)}^\infty \left[\frac{r - t(RH)}{r}\right]^3 \phi_{por}^{pdf}(r)\,\mathrm{d}r, \tag{25}$$

where the term in brackets accounts for the adsorbed water layers, see Fig. 4. Notably, both the lower integration limit, r_{lg}, and the thickness of the adsorbed water layer, t, are nonlinear functions of the relative humidity, see Eqs. (10) and (9). The symbol $\phi_{por}^{pdf}(r)$ denotes the pore size probability distribution function of all pores. The latter results from superposition of the pore size probability distribution functions of the gel and the capillary pores, see Eq. (21), as

$$\phi_{por}^{pdf}(r) = \frac{f_{gpor}^{por}}{R_{gpor}}\exp\left(-\frac{r}{R_{gpor}}\right) + \frac{f_{cpor}^{por}}{R_{cpor}}\exp\left(-\frac{r}{R_{cpor}}\right), \tag{26}$$

where f_{gpor}^{por} and f_{cpor}^{por} denote the volume fractions of the gel and the capillary pores, respectively, with regard to the total pore volume. These two quantities can be directly derived from the hydration model, Eqs. (6)–(8), as

$$f_{gpor}^{por} = \frac{f_{gpor}^{cp}}{f_{gpor}^{cp} + f_{cpor}^{cp}} = \frac{0.19\,\xi}{w/c - 0.17\,\xi},$$
$$f_{cpor}^{cpor} = \frac{f_{cpor}^{cp}}{f_{gpor}^{cp} + f_{cpor}^{cp}} = \frac{w/c - 0.36\,\xi}{w/c - 0.17\,\xi}, \tag{27}$$

where $f_{gpor}^{cp} = f_{hf}^{cp}\, f_{gel}^{hf}\, f_{gpor}^{gel}$ and $f_{cpor}^{cp} = f_{hf}^{cp}\, f_{cpor}^{hf}$, see Eqs. (6)–(8). Combining Eqs. (23)–(27), and considering that r_{lg} in Eq. (25) is a function of the relative humidity, see Eq. (10), allows for expressing the model-predicted saturation ratio S_r^{mod} as a function of the relative humidity RH and the characteristic pore radii R_{gpor} and R_{cpor}. The latter are identified in the following.

Many experimental adsorption isotherms were fitted by Brunauer et al. [32,57], using the following function

$$S_r^{\exp} = \frac{RH(1-k)[1 + k(C-1)]}{(1 - k\ RH)[1 + k\ RH(C-1)]}. \tag{28}$$

For cementitious materials, semi-empirical formulae for C and k were established by Xi et al. [33]:

$$C = \exp\left(\frac{855\ \mathrm{K}}{T}\right), \quad k = \frac{(1 - 1/n)\,C - 1}{C - 1}, \tag{29}$$

where K stands for the SI unit Kelvin, and n is a function of the age t of the material and of its initial water-to-cement mass ratio w/c, which reads as

$$n = \left(2.5 + \frac{15\ \mathrm{d}}{t}\right)(0.33 + 2.2\ w/c)\ N_{ct},$$
$$t > 5\ \mathrm{d},\ 0.3 < w/c < 0.7, \tag{30}$$

where d stands for the physical unit day. Finally, N_{ct} is equal to 1.1 for type I Portland cement.

The characteristic pore radii R_{gpor} and R_{cpor} are identified by minimization of the square root of the sum of the squared errors, ε_{SRSS}, quantifying the difference between saturation degrees derived from the pore size distribution model, see S_r^{mod} in Eq. (23), and from adsorption isotherms, see $S_r^{\exp}$ in Eq. (28),

$$\varepsilon_{SRSS}(R_{gpor}, R_{cpor}) = \sqrt{\frac{1}{99}\sum_{i=1}^{99}[S_r^{mod}(RH_i, R_{gpor}, R_{cpor}) - S_r^{\exp}(RH_i)]^2}$$
$$\rightarrow \min, \tag{31}$$

where $RH_i = i/100$. The optimization problem Eq. (31) is solved numerically using continuously refined search intervals, as detailed in Ref. [58]. Optimal characteristic radii of the gel and the capillary pores are identified for mature cement pastes with initial water-to-cement mass ratios $w/c \in [0.40; 0.70]$, made of type I Portland cement, cured at room temperature ($T = 293.15$ K) for 90 days ($\xi \approx 0.8$) [43], such that $\gamma^{lg} = 0.07275\ \mathrm{N\,m^{-1}}$ [20] and $\rho_{H_2O} = 998.2067\ \mathrm{kg\,m^{-3}}$ [46], see Table 2. The identified pore radii result in a very good agreement between the model-predicted adsorption isotherms and the Brunauer-Xi-type counterparts, see the error values ε_{SSRS} listed in Table 2 and Fig. 5 (a). In addition, the identified values of R_{gpor} and R_{cpor} are close to 2 nm

Table 2
Volume fractions and characteristic radii of gel and capillary pores of mature cement pastes with initial water-to-cement mass ratios $w/c \in [0.40; 0.70]$, cured at room temperature ($T = 293.15$ K) for 90 days ($\xi = 0.80$), such that $\gamma^{lg} = 0.07275\ \mathrm{N\,m^{-1}}$ and $\rho_{H_2O} = 998.2067\ \mathrm{kg\,m^{-3}}$.

w/c	f_{gpor}^{por} [−]	R_{gpor} [nm]	f_{cpor}^{por} [−]	R_{cpor} [nm]	ε_{SSRS} [−]
0.40	0.5757	1.9871	0.4243	12.6600	0.00883
0.45	0.4841	1.9211	0.5159	11.4390	0.01122
0.50	0.4177	1.9149	0.5823	11.1144	0.01299
0.55	0.3671	1.9446	0.6329	11.1467	0.01427
0.60	0.3275	1.9986	0.6725	11.3568	0.01523
0.65	0.2957	2.0701	0.7043	11.6675	0.01596
0.70	0.2695	2.1549	0.7305	12.0399	0.01653

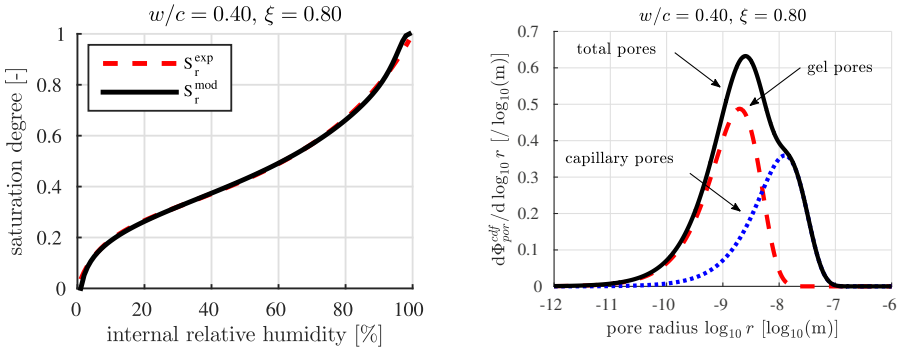

Fig. 5. Results from identification of characteristic pore sizes, carried out for mature cement paste with initial water-to-cement mass ratio of 0.40, cured at room temperature ($T = 293.15$ K) for 90 days ($\xi = 0.80$), determined from the pore size distribution model, see Eqs. (23)–(27), and from the adsorption isotherms, see Eqs. (28)–(30), considering the following values of the surface tension and the water mass density: $\gamma^{lg} = 0.07275\,\mathrm{N\,m^{-1}}$, $\rho_{H_2O} = 998.2067\,\mathrm{kg\,m^{-3}}$: (a) saturation degree as a function of the relative humidity in the air-filled pores, and (b) cumulative size-distribution functions of pores.

and 12 nm, respectively. This is in very good agreement with previous studies [15], which were also based on sorption isotherms. The cumulative pore size distribution function $\Phi_{por}^{cdf}(r)$, representing the integral of the pore size probability distribution function Eq. (26) over the pore radius, reads as

$$\Phi_{por}^{cdf}(r) = f_{gpor}^{por}\left[1-\exp\left(-\frac{r}{R_{gpor}}\right)\right] + f_{cpor}^{por}\left[1-\exp\left(-\frac{r}{R_{cpor}}\right)\right]. \tag{32}$$

It is well suited to illustrate the identified pore size distributions, see Fig. 5 (b).

Based on the identified pore radii R_{gpor} and R_{cpor}, the average effective pore pressures p_{gpor} and p_{cpor} can be quantified for any value of the internal relative humidity RH and any temperature T, see Eqs. (22), (20), and (9). Returning to the hierarchical organization of cement pastes as illustrated in Fig. 3, the average effective pore pressures are to be upscaled to the macroscopic scale of cement pastes.

2.5. Hygrothermoporoelastic homogenization of mature cement pastes

The microstructure of mature cement pastes is subdivided into three matrix-inclusion composites, see Fig. 3. This renders the Mori-Tanaka scheme appropriate for analytical homogenization of poroelastic properties [26,36,37,59,60,81]. It allows for analytical homogenization of poroelastic properties in the framework of microporomechanics [60]. Each representative volume element (RVE) with volume V_{RVE} is subdivided into a matrix phase and an inclusion phase, occupying the domains V_m and V_i, respectively. Both material phases $k \in [m;i]$ exhibit a specific elastic stiffness $\mathbb{C}_k$, a specific eigenstress $\boldsymbol{\sigma}_k^E$, and a known volume fraction f_k:

$$\forall\, \underline{x} \in V_k\colon \begin{cases} \mathbb{C}(\underline{x}) = \mathbb{C}_k \\ \boldsymbol{\sigma}^E(\underline{x}) = \boldsymbol{\sigma}_k^E \end{cases}, \quad f_k = \frac{V_k}{V_{RVE}}, \quad k \in [m;\, i]. \tag{33}$$

The generalized Hooke's law of the homogenized composite follows from Levin's theorem [61], containing the macroscopic stress $\boldsymbol{\Sigma}$, the macroscopic strain $\mathbf{E}$, the homogenized stiffness $\mathbb{C}_{\mathrm{hom}}$, and the homogenized eigenstress $\boldsymbol{\Sigma}_{\mathrm{hom}}^E$ [26,61]:

$$\boldsymbol{\Sigma} = \mathbb{C}_{\mathrm{hom}}\colon \mathbf{E} + \boldsymbol{\Sigma}_{\mathrm{hom}}^E, \tag{34}$$

$$\mathbb{C}_{\mathrm{hom}} = f_m \mathbb{C}_m\colon \mathbb{A}_m + f_i \mathbb{C}_i\colon \mathbb{A}_i, \tag{35}$$

$$\boldsymbol{\Sigma}_{\mathrm{hom}}^E = f_m \boldsymbol{\sigma}_m^E\colon \mathbb{A}_m + f_i \sigma_i^E\colon \mathbb{A}_i, \tag{36}$$

where $\mathbb{A}_m$ and $\mathbb{A}_i$ are the phase strain concentration tensors of the two material phases, and symbol ":" refers to second-order tensor contraction. Mori-Tanaka estimates of these two tensors read as [37,59]

$$\mathbb{A}_k = [\mathbb{I} + \mathbb{S}\colon \mathbb{C}_m^{-1}\colon (\mathbb{C}_k - \mathbb{C}_m)]^{-1}\colon \left[\sum_{j=m,i} f_j [\mathbb{I} + \mathbb{S}\colon \mathbb{C}_m^{-1}\colon (\mathbb{C}_j - \mathbb{C}_m)]^{-1}\right]^{-1}, \quad k \in [m;\, i], \tag{37}$$

where $\mathbb{S}$ is the Eshelby tensor of a spherical inclusion embedded in an infinite matrix of stiffness $\mathbb{C}_m$, defined as [62]

$$\mathbb{S} = S_{vol}\, \mathbb{I}_{vol} + S_{dev}\, \mathbb{I}_{dev}, \tag{38}$$

$$S_{vol} = \frac{3\, k_m}{3\, k_m + 4\, \mu_m}, \tag{39}$$

$$S_{dev} = \frac{6(k_m + 2\, \mu_m)}{5(3\, k_m + 4\, \mu_m)}. \tag{40}$$

The homogenized stiffness tensor is obtained from inserting Eq. (38) into Eq. (37), followed by substituting the result together with Eq. (4) into Eq. (35):

$$\mathbb{C}_{\mathrm{hom}} = 3\, k_{\mathrm{hom}}\, \mathbb{I}_{vol} + 2\, \mu_{\mathrm{hom}}\, \mathbb{I}_{dev}, \tag{41}$$

with

$$k_{\mathrm{hom}} = \frac{f_i\, k_i \left(1 + \frac{S_{vol}\,(k_i - k_m)}{k_m}\right)^{-1} + f_m\, k_m}{f_i \left(1 + \frac{S_{vol}\,(k_i - k_m)}{k_m}\right)^{-1} + f_m}, \tag{42}$$

$$\mu_{\mathrm{hom}} = \frac{f_i\, \mu_i \left(1 + \frac{S_{dev}\,(\mu_i - \mu_m)}{\mu_m}\right)^{-1} + f_m\, \mu_m}{f_i \left(1 + \frac{S_{dev}\,(\mu_i - \mu_m)}{\mu_m}\right)^{-1} + f_m}. \tag{43}$$

where k_{hom} and μ_{hom} are the homogenized bulk and shear moduli of the composite. The homogenized eigenstress follows from consideration of isotropic phase eigenstresses $\boldsymbol{\sigma}_p^E = -p_p \boldsymbol{1}$, with index $p \in [m;i]$. Inserting Eq. (38) into Eq. (37) and substituting the result into Eq. (36) gives

$$\boldsymbol{\Sigma}_{\mathrm{hom}}^E = -p_{\mathrm{hom}}\, \boldsymbol{1}, \tag{44}$$

with

$$p_{\mathrm{hom}} = p_m\, B_m + p_i\, B_i, \tag{45}$$

and

$$B_m = \frac{f_m}{f_m + f_i \left[1 + \frac{S_{vol}\,(k_i - k_m)}{k_m}\right]^{-1}}, \tag{46}$$

$$B_i = \frac{f_i}{\left(1 + \frac{S_{vol}\,(k_i - k_m)}{k_m}\right)\left\{f_m + f_i \left[1 + \frac{S_{vol}\,(k_i - k_m)}{k_m}\right]^{-1}\right\}}. \tag{47}$$

In order to homogenize the thermal expansion of cement pastes, analytical upscaling of the elastic stiffness, see Eqs. (41)–(43), and of the eigenstress, see Eqs. (44)–(47), is carried out, in three subsequent

Table 3
Step-by-step homogenization of mature cement pastes, subdivided into homogenization of the hydrate gel, the hydrate foam, and the cement paste, see also Fig. 3.

	Constituents	Volume fraction	Stiffness	Eigenstress	Homog. stiffness	Homog. eigenstress
Hydrate gel	Solid hydrates	f_{hyd}^{gel} *	$\mathbb{C}_{hyd}$ †	$\boldsymbol{\sigma}_{hyd}^{E} = -\mathbb{C}_{hyd}\colon \alpha_{hyd}\Delta T\boldsymbol{1}$	$\mathbb{C}_{gel}$ §	$\boldsymbol{\Sigma}_{gel}^{E}$ ¶
	Gel pores	f_{gpor}^{gel} *	$\mathbb{C}_{gpor} = 0$	$\boldsymbol{\sigma}_{gpor}^{E} = -p_{gpor}\boldsymbol{1}$ ‡		
Hydrate foam	Hydrate gel	f_{gel}^{hf} *	$\mathbb{C}_{gel}$	$\boldsymbol{\Sigma}_{gel}^{E}$	$\mathbb{C}_{hf}$ §	$\boldsymbol{\Sigma}_{hf}^{E}$ ¶
	Capillary pores	f_{cpor}^{hf} *	$\mathbb{C}_{cpor} = 0$	$\boldsymbol{\sigma}_{cpor}^{E} = -p_{cpor}\boldsymbol{1}$ ‡		
Cement paste	Hydrate foam	f_{hf}^{cp} *	$\mathbb{C}_{hf}$	$\boldsymbol{\Sigma}_{hf}^{E}$	$\mathbb{C}_{cp}$ §	$\boldsymbol{\Sigma}_{cp}^{E}$ ¶
	Clinker	f_{clin}^{cp} *	$\mathbb{C}_{clin}$ †	$\boldsymbol{\sigma}_{clin}^{E} = -\mathbb{C}_{clin}\colon \alpha_{clin}\Delta T\boldsymbol{1}$		

* See Eqs. (6)–(8).
† See Eqs. (4) and (5).
‡ See Eqs. (22), (20), and (9).
§ See Eqs. (41)–(43), as well as Eqs.(39) and (40).
¶ See Eqs. (44)–(47), as well as Eqs.(39) and (40).

steps, for the matrix-inclusion composites of the cement pastes shown in Fig. 3. For the inputs and the homogenization results, see Table 3. To this end, *free* thermal expansion of cement paste is considered, i.e. $\boldsymbol{\Sigma}_{cp} = 0$. Inserting the vanishing macrostress into Eq. (34) yields, after solving for the macrostrain $\mathbf{E}_{cp}$, the macroscopic eigenstrain $\mathbf{E}_{cp}^{E}$ as

$$\mathbf{E}_{cp}^{E}(T, RH) = -\mathbb{C}_{cp}^{-1}\colon \boldsymbol{\Sigma}_{cp}^{E}(T, RH). \tag{48}$$

The thermal expansion coefficient of cement paste is proportional to the hygrothermic eigenstrain difference, quantified for a temperature difference ΔT, i.e.

$$\alpha_{cp}\,\Delta T\,\boldsymbol{1} = \mathbf{E}_{cp}^{E}(T + \Delta T, RH + \Delta T{\cdot}\Delta RH/\Delta T) - \mathbf{E}_{cp}^{E}(T, RH). \tag{49}$$

Herein, $T = 293.15$ K and $\Delta T = 1$ K are considered, for corresponding values of the surface tension $\gamma^{\ell g}$ and the mass density of water ρ_{H_2O}, see Table 1. In addition, the change of the internal relative humidity resulting from a temperature change is taken into account, see the first term on the right-hand-side of Eq. (49).

2.6. Identification of the solid expansion coefficient

In order to identify the unknown thermal expansion coefficients of hydrates and clinker, see Table 3, they are assumed to be equal, i.e. $\alpha_{hyd} = \alpha_{clin}$. They are identified by means of the thermal expansion coefficients measured on fully dried cement pastes, i.e. $RH = 0\%$. In this context, the temperature variation is considered to result in thermal dilatation of the solid constituents, while the average effective pore pressures remain constant. Consequently,

$$\alpha_{hyd} = \alpha_{clin} = 12.5{\cdot}10^{-6}\ \mathrm{K}^{-1}, \tag{50}$$

see Fig. 1. The proof that the homogenized thermal expansion coefficient of the matrix-inclusion composites in Fig. 3 is equal to that of the solids, see Eq. (50), is given in Appendix B. For a more refined approach, which abandons the assumption of $\alpha_{hyd} = \alpha_{clin}$, see Appendix C.

2.7. Identification of hygrothermic coefficients of cement pastes with $w/c = 0.40$ and $\xi = 0.80$

The homogenization approach described in Section 2.5 is used for identification of hygrothermic coefficients. The resulting inverse problem is solved for relative humidities $RH \in [20\%; 85\%]$. For each value of the relative humidity, the hygrothermic coefficient $\Delta RH/\Delta T$ is determined such that the homogenized thermal expansion coefficient α_{cp}, see Eq. (49), is equal to the value of the experimental master curve, see Fig. 1 and the regression function in Eq. (3). The identified hygrothermic coefficients form an asymmetrical bell-shaped function of the internal relative humidity which prevails in the air-filled pores just before the temperature change, see Fig. 6. The results from the identification agree well with measurement results by Nilsson [17] and Grasley [10], see Fig. 6.

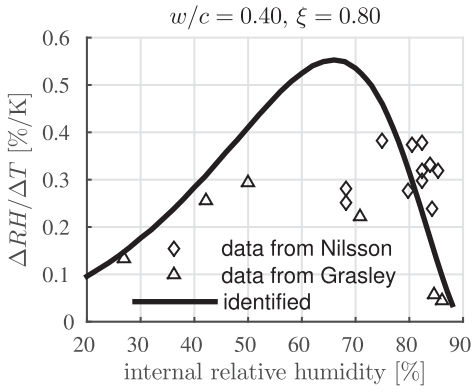

Fig. 6. Identified hygrothermic coefficient $\Delta RH/\Delta T$ as a function of the relative humidity, identified with the developed multiscale model from the "master-curve" of the thermal expansion coefficient, see Eq. (3) and Fig. 1, and test results by Nilsson [17] and Grasley [10] for mature cement pastes with initial water-to-cement mass ratio of 0.40.

2.8. Identification of the water uptake/release by hydration products as a function of the internal relative humidity and temperature change

Thermal expansion of cement paste occurs on the way to a uniform temperature distribution inside a tested specimen. Such a process takes typically from several minutes to a few hours, depending on the size of the specimen and on the magnitude of the temperature change. It is significantly *shorter* than the period of time required to balance the internal and the external relative humidities, prevailing inside and around partially saturated and drained cement paste samples. This balance requires a significant water transport through the pore network and frequently takes several weeks. Based on this "separation of time scales"-argument, it is concluded that the water mass exchange between the cement paste specimens and their exterior environment is insignificant as regards characterization of thermal expansion coefficients, so that the cement pastes may be treated as closed systems, referred to in poromechanics as "sealed conditions". Consequently, mass conservation can be considered as the basis for quantifying the water uptake/release by the hydration products.

A temperature increase results in an increase of the internal relative humidity, see Fig. 2, and this yields both an increase of the thickness of the adsorbed water layer, see Eq. (9), and an increase of the radius $r_{\ell g}$, see Eq. (10). Both effects underline that the volume of liquid water (both adsorbed water and bulk water) increases. Using the presented model, this cannot be explained by regular or anomalous thermal expansion of water alone, see Section 4.3. Given that the overall mass of the cement paste is constant (= mass conservation, see above) and,

thus, that the total mass of water is constant, it is concluded that the hydration products act as a water source, i.e. they release water

$$\Delta m_{hyd} = m^{liq}_{H_2O}(T + \Delta T,\, RH + \Delta T{\cdot}\Delta RH/\Delta T) - m^{liq}_{H_2O}(T,\, RH), \tag{51}$$

where $m^{liq}_{H_2O}$ can be calculated using the developed multiscale poromechanics model, see Eqs. (24)–(27), under consideration that $r_{\ell g}$ in Eq. (25) is a nonlinear function of the relative humidity and of the temperature, see Eq. (10). Notably, the change of the mass of water vapor is by orders of magnitude smaller than the change of the mass of liquid water. Therefore, water vapor was disregarded in Eq. (51). Finally, the dimensionless "specific water uptake/release" of solid hydrates, $\Delta\mu$, is introduced as the mass loss of the solid hydrates, see Eq. (51), divided by their initial mass, m_{hyd}, delivering

$$\Delta\mu = \frac{\Delta m_{hyd}}{m_{hyd}}, \tag{52}$$

with

$$m_{hyd} = \rho_{hyd}\, V_{hyd}, \tag{53}$$

where $\rho_{hyd} = 2.85 \cdot 10^3\,\mathrm{kg\,m^{-3}}$ [29] denotes the mass density of the solid hydrates. The initial volume of solid hydrates, V_{hyd}, is expressed, by analogy to Eq. (24), through the pore volume V_{por} as

$$V_{hyd} = V_{por}\,\frac{f^{cp}_{hyd}}{f^{cp}_{por}} = V_{por}\,\frac{0.49\,\xi}{w/c - 0.17\,\xi}, \tag{54}$$

with $f^{cp}_{hyd} = f^{gel}_{hyd}\, f^{hf}_{gel}\, f^{cp}_{hf}$ and $f^{cp}_{por} = f^{gel}_{gpor}\, f^{hf}_{gel}\, f^{cp}_{hf} + f^{hf}_{cpor}\, f^{cp}_{hf}$, see Eqs. (6)–(8).

The water uptake/release coefficient $\Delta\mu/\Delta T$ is identified based on the following expression, resulting from the combination of Eqs. (51)–(54) with Eqs. (24) and (25):

$$\begin{aligned}\frac{\Delta\mu}{\Delta T} = {} & \frac{(w/c - 0.17\xi)\,\rho_{H_2O}(T + \Delta T)}{0.49\,\xi\,\Delta T\,\rho_{hyd}} \\ & \times\left\{1 - \int_{r_{\ell g}(T+\Delta T, RH+\Delta RH)}^{\infty}\left[\frac{r - t(RH + \Delta RH)}{r}\right]^3 \phi^{pdf}_{por}(r)\mathrm{d}r\right\} \\ & - \frac{(w/c - 0.17\,\xi)\,\rho_{H_2O}(T)}{0.49\,\xi\,\Delta T\,\rho_{hyd}}\left\{1\right. \\ & \left. - \int_{r_{\ell g}(T, RH)}^{\infty}\left[\frac{r - t(RH)}{r}\right]^3 \phi^{pdf}_{por}(r)\mathrm{d}r\right\},\end{aligned} \tag{55}$$

see also Eqs. (9) and (10) for the definition of t and $r_{\ell g}$, respectively. Considering, in Eq. (55), a temperature increase from $T = 293.15\,\mathrm{K}$ to $T + \Delta T = 294.15\,\mathrm{K}$, the corresponding values of ρ_{H_2O}, ν_m, and $\gamma^{\ell g}$ according to Table 1, $w/c = 0.40$ and $\xi = 0.80$, as well as the identified hygrothermic coefficients illustrated in Fig. 6, the water uptake/release coefficient $\Delta\mu/\Delta T$ is identified. It forms an asymmetrical bell-shaped function of the internal relative humidity which prevails in the air-filled pores just before the temperature change, see Fig. 7. The maximum of $\Delta\mu/\Delta T$ amounts to $6.2 \cdot 10^{-4}\,\mathrm{K^{-1}}$ and refers to the internal relative humidity $RH = 72\%$. The characteristic order of magnitude of water uptake/release coefficients underlines that the exchange between solid and liquid water is a rather subtle effect, but still large enough as to result in significant hygrothermic coefficients and in the thermal expansion coefficients illustrated in Fig. 1.

3. Bottom-up prediction of hygrothermic coefficients and thermal expansion coefficients of cement pastes with $w/c \in [0.50; 0.60; 0.70]$

The water uptake/release coefficients (Fig. 7) represent a material property of solid hydrates. Therefore, they are valid for *all* Portland cement pastes, irrespective of their composition, and not only for

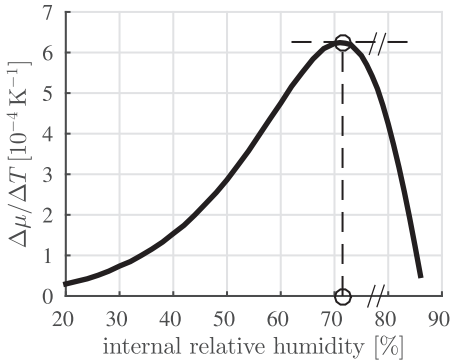

Fig. 7. Identified specific water uptake/release by hydration products per unit temperature increase, referred to as "water uptake/release coefficients", see Eq. (55).

$w/c = 0.40$, for which the top-down analysis was carried out. In order to prove the mixture-independence of the water uptake/release coefficients exemplarily, a bottom-up approach is applied to cement pastes with $w/c = [0.50; 0.60; 0.70]$. The aim is to *predict* hygrothermic coefficients and thermal expansion coefficients of cement pastes, and to compare them with experimental data that were not involved in the identification of the water uptake/release coefficients.

3.1. Prediction of hygrothermic coefficients of mature cement pastes with different initial water-to-cement mass ratios

Hygrothermic coefficients are predicted on the basis of mass conservation, as explained in Section 2.8. They follow from the water uptake/release coefficients shown in Fig. 7 and from the developed pore size distribution model, see Eqs. (26)–(27) and Table 2. The predicted hygrothermic coefficients form similarly shaped asymmetrical bell-shaped functions which are the smaller, the larger the initial water-to-cement mass ratio, see Fig. 8. The quantitative differences can be explained by the fact that the porosity of mature cement pastes increases with increasing initial water-to-cement mass ratio. As for regression functions rendering model predictions accessible, see Appendix D.

As for the exemplary validation, the hygrothermic coefficients predicted for $w/c = 0.50$, are compared with experimental data from Persson [18], Radjy [19], and Grasley [10], who tested mature cement pastes with $w/c \in [0.48; 0.50]$. Given that measured hygrothermic coefficients exhibit a rather large intrinsic experimental uncertainty, the obtained agreement is satisfactory, see Fig. 9. This corroborates that the identified water uptake/release coefficients (Fig. 7) are indeed a material property of solid hydrates.

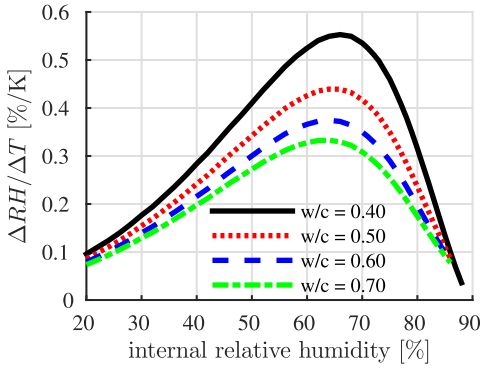

Fig. 8. Model predicted hygrothermic coefficients of mature cement pastes with initial water-to-cement mass ratios of 0.40, 0.50, 0.60, and 0.70 and hydration degree $\xi = 0.80$.

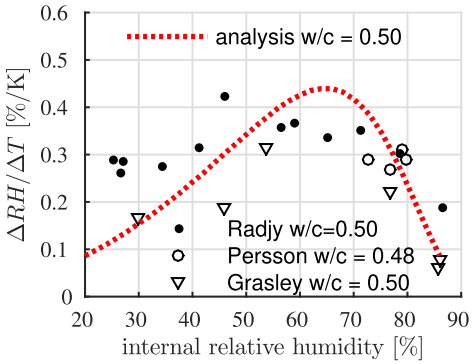

Fig. 9. Comparison of hygrothermic coefficients, measured by Grasley [10], Persson [18], and Radjy et al. [19], with model predictions for mature cement paste with an initial water-to-cement mass ratio of 0.50 and hydration degree $\xi = 0.80$.

3.2. Prediction of thermal expansion coefficients of mature cement pastes with different initial water-to-cement mass ratios

Thermal expansion coefficients of cement pastes are predicted by using the hygrothermic coefficients shown in Fig. 8 as input for the developed multiscale poroelastic model, see Eqs. (1)–(49) and Table 3. The predicted thermal expansion coefficients form a dense bunch of similarly shaped asymmetrical bell-shaped functions. Quantitatively, they exhibit only very small fluctuations for initial water-to-cement mass ratio in the range from 0.12 to 0.70, see Fig. 10.

In the context of the exemplary validation, it is remarkable that the thermal expansion coefficients predicted for initial water-to-cement mass ratios in the interval $w/c \in [0.40; 0.70]$ are very close to the master curve of Eq. (3), which reproduces experimental measurements on pastes with w/c-values in the non-overlapping interval [0.12; 0.40]. In addition, the model predictions are compared with measured thermal expansion coefficients of Grasley [10], which were not included in Fig. 1 and, therefore, neither contributed to the master curve of Eq. (3), nor to the identification of the water uptake/release coefficients. The agreement between the model predictions and the experimental data is again satisfactory, see Fig. 10. This further corroborates that the identified water uptake/release coefficients (Fig. 7) are indeed a mixture-independent material property of hydration products.

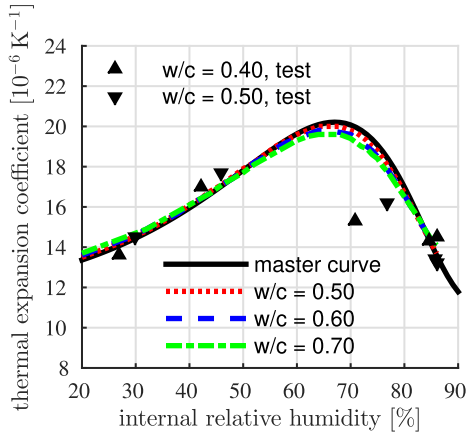

Fig. 10. Dependence of the thermal expansion coefficient on the internal relative humidity: model prediction for mature cement paste with w/c of 0.50, 0.60, and 0.70 and with $\xi = 0.80$, master-curve for mature cement paste with $w/c = 0.12 \sim 0.40$; and test results from Grasley et al. [10] for mature cement pastes with w/c of 0.40 and 0.50.

4. Discussion

Redistribution of *liquid* water within the microstructure of cement pastes is standardly considered to govern thermohygroporomechanical phenomena with characteristic duration from a few seconds to several hours. This dates back to Powers [41,63], who proposed (i) that short-term mechanical or thermal loading of partially saturated concrete disturbs the free-energy equilibrium, such that water redistributes within nanoscopic pores of different sizes, and (ii) that this migration of water results in considerable macroscopic deformation of concrete. This idea has motivated many follow-up research activities related to both modeling and experimentation, see Refs.[2,64-66] and [10,17-19,21,67]. However, the built-up of pore pressure resulting from a temperature increase of *liquid-saturated* cement pastes cannot be explained by redistribution of liquid water. Therefore, it was related to an anomalous thermal expansion of water [68-70]. The proposed quasi-instantaneous water uptake/release by the hydration products, in turn, can explain both the redistribution of liquid water under partially saturated conditions and the pressurization of pore water upon increasing the temperature under liquid-saturated conditions.

Water uptake/release by hydration products was so far mainly considered in the context of long-term sorption processes with characteristic duration from several days to several weeks. Related research focuses particularly on calcium-silicate-hydrates (C-S-H), i.e. on the most important type of cement hydrates. Despite very intensive research activities, the molecular composition of C-S-H is not yet fully understood. As regards the water content of C-S-H, ongoing discussions refer to typical chemical compositions ranging, e.g. from 1.7 $CaO \cdot SiO_2 \cdot 1.8\ H_2O$, as quantified by small angle scattering techniques [28], to 1.7 $CaO \cdot SiO_2 \cdot 1.3\ H_2O$, as determined by means of gravimetry for d-dried C-S-H [29]. These two exemplary formulae underline that the water content of C-S-H is variable, at least during long-term sorption experiments.

Herein, it was essentially proposed that the water uptake/release by the hydration products is not necessarily a very slow process. It appears to be actually fast enough to be the origin of quasi-instantaneous water redistributions, associated with short-term thermohygroporomechanical phenomena. This idea is consistent with the polymerization of mature cement paste under room temperature [71-73], where chemical bonds between silicon atoms and hydroxyl groups change upon a moderate temperature increase such that the liquid water is set free, i.e.

$$-\mathrm{Si}-\mathrm{OH} + \mathrm{HO}-\mathrm{Si}- \Longrightarrow -\mathrm{Si}-\mathrm{O}-\mathrm{Si}- + \mathrm{H_2O}. \quad (56)$$

Also, water uptake/release by hydrates is reminiscent of quasi-instantaneous changes of internal relative humidity resulting from mechanical loading of cement pastes, as described by Wyrzykowski and Lura [67]. In addition, evidence of some fast water redistribution was reported by Gajewicz et al. [74], in the context of ^{1}H NMR relaxometry investigation of gel-pore drying shrinkage in cement pastes.

4.1. Temperature-driven water uptake/release by hydrates: a first direct experimental evidence provided by Wyrzykowski et al. [27]

After submission of the original version of the present manuscript, our idea of the hydrates taking up/releasing water upon temperature changes, was strongly supported by direct experimental evidence [27]. Proton nuclear magnetic resonance (^{1}H NMR) studies of mature cement pastes [27] showed heating-induced transport of water from the C-S-H interlayers to the gel/capillary porosities, and vice versa. The observed water redistribution process has the following characteristics:

1. quasi-instantaneous nature and full reversibility,
2. independence of the initial water-to-cement mass ratio, at least within the investigated interval of $w/c \in [0.25; 0.50]$, and
3. dependence on the internal relative humidity prevailing inside the

air-filled pores right before the temperature change, with the maximum water exchange taking place around $RH = 75\%$.

In addition, the observed water redistribution process was *conceptually* coupled to both hygrothermic effects and thermal expansion of mature cement pastes [27].

In the present paper, values of cooling/heating-driven uptake/release of water by hydrates are identified for mature cement pastes, utilizing top-down multiscale analysis. Thereby, uptake/release of water by hydrates was

1. assumed to be a quasi-instantaneous and fully reversible process,
2. found to be universal in the sense of being independent of the initial water-to-cement mass ratio, at least in the studied interval of $w/c \in [0.40; 0.70]$, and
3. found to be a nonlinear function of the internal relative humidity prevailing inside the air-filled pores right before the temperature change, with the maximum intensity around $RH = 72\%$.

In addition, the water redistribution process was linked *quantitatively* both to hygrothermic coefficients and to thermal expansion coefficients of mature cement pastes.

The previous two paragraphs underline that two independent methods, a theoretical method based on multiscale micro-poromechanics and an experimental method based on ^{1}H NMR [27] have led to virtually the same conclusions. This supports the idea of water uptake/release by hydrates as the mechanism governing hygrothermic coefficients and thermal expansion of cement paste, particularly so within the herein studied interval of $RH \in [25\%; 85\%]$.

4.2. Additional mechanism: rearrangements of the nanostructure

Considering the water uptake/release by hydration products as the origin of hygrothermic coefficients, delivers a satisfactory description of the thermal expansion of mature cement paste in the important range of the relative humidity from 25% to 85%. The regimes of very small and very large relative humidities have not been explored herein. In these regimes, rearrangements of the nanostructure of cement pastes are likely to take place:

- At very small relative humidities ($RH < 20\%$), nanostructural transformations may not only comprise removal of interlayer water from C-S-H, as concluded from isothermal sorption experiments [29,75], but also rearrangement of the C-S-H sheets themselves, as concluded from ^{1}H NMR measurements [74].
- At very large relative humidities ($RH > 85\%$), individual calcium silicate sheets, positioned at the surface of layered calcium-silicate-hydrates, may detach from the rest and bend into the adjacent gel pore, subdividing the latter into two smaller pores [27].

These microstructural rearrangements may give rise to hygrothermic coefficients which are significantly larger than the ones identified in the present paper, compare the experimental values reported in Figs. 6, 8, and 9, referring to the range from 85% to 90%, with the results of the measurements performed by Wyrzykowski and Lura [21]. In this context, it is also noteworthy that Wyrzykowski and Lura [21] studied *young* cement pastes, with material ages ranging from 1 day to 7 days, produced with initial water-to-cement mass ratios ranging from 0.22 to 0.35, and tested under relative humidities ranging from 86% to 98%. Herein, the study focused on *mature* cement pastes, with material ages amounting up to 6 months, produced with initial water-to-cement mass ratios ranging from 0.40 to 0.50, and tested under relative humidities ranging from some 25% to some 85%. This underlines that the two studies do neither overlap in terms of material composition nor in terms of material age, and that the overlap in terms of the test conditions is very small (if at all existing).

4.3. Additional mechanism: anomalous expansion of liquid pore water

Consideration of water uptake/release by hydrates allows for explaining hygrothermic coefficients in the interval of $RH \in [25\%; 85\%]$, of several mature cement pastes, differing in the initial water-to-cement mass ratio. Another mechanism that is quite frequently discussed in this context, is anomalous thermal expansion of confined, rather than bulk, pore water [69]. This is the motivation to show how much of the overall hygrothermic coefficient of cement paste is simply due to thermal expansion of the pore water, and how much this share would depend on whether the thermal expansion coefficient of pore water would be that of bulk water or that of confined water.

The thermal expansion coefficient of bulk water, $\alpha_{H_2O}^{bulk}$, is associated with the temperature-dependent densities of bulk water, as given in Table 1 for mass density values at 293.15 K and 294.15 K. Namely, mass conservation of expanding water implies that

$$\rho_{H_2O}(273.15\ \mathrm{K})V_{H_2O}(273.15\ \mathrm{K}) = \rho_{H_2O}(274.15\ \mathrm{K})V_{H_2O}(274.15\ \mathrm{K}) = const.\ , \tag{57}$$

whereby the relation between the volumes $V_{H_2O}(273.15\ \mathrm{K})$ and $V_{H_2O}(274.15\ \mathrm{K})$ reads as

$$V_{H_2O}(274.15\ \mathrm{K}) = V_{H_2O}(273.15\ \mathrm{K})(1 + \alpha_{H_2O}^{bulk}\cdot 1\mathrm{K})^3. \tag{58}$$

The thermal expansion coefficient of bulk water follows from inserting Eq. (58) into Eq. (57), solving the resulting expression for $\alpha_{H_2O}^{bulk}$, and specializing the result for the numerical values of the mass densities $\rho_{H_2O}(273.15\ \mathrm{K})$ and $\rho_{H_2O}(274.15\ \mathrm{K})$, given in Table 1, as

$$\alpha_{H_2O}^{bulk} = 70.70\cdot 10^{-6}\ \mathrm{K}^{-1}. \tag{59}$$

This is significantly larger than the thermal expansion coefficient of the solid constituents of cement paste, see Eq. (50) and Table C.4. In order to demonstrate the contribution of the thermal expansion of bulk pore water to the hygrothermic coefficients, the mathematical term associated with water uptake/release by hydrates is set equal to zero:

$$\frac{\Delta\mu}{\Delta T} = 0. \tag{60}$$

Thus, the mass of liquid water, both adsorbed water and bulk water, is constant:

$$m_{H_2O}^{liq}(T, RH) = m_{H_2O}^{liq}(T + \Delta T, RH + \Delta T\cdot\Delta RH/\Delta T). \tag{61}$$

The mass of liquid pore water is quantified based on Eq. (24), considering the temperature-dependent mass density of water (Table 1) and the volume fraction of air according to Eq. (25). Values of the hygrothermic coefficient are quantified, as the temperature increases from $T = 293.15\ \mathrm{K}$ to $T + \Delta T = 294.15\ \mathrm{K}$, see the dashed line in Fig. 11. It is concluded that consideration of the thermal expansion of bulk pore water alone cannot explain the experimentally measured hygrothermic coefficients.

Anomalously larger thermal expansion is reported for pore water, confined in pores smaller than 15 nm [76]. This anomalous thermal expansion increases with decreasing size of the pores and ranges, at room temperature, from 1 to 3 times the thermal expansion of unconfined bulk water [76]

$$\alpha_{H_2O}^{conf} \in [70.70\cdot 10^{-6}\ \mathrm{K}^{-1};\ 212.10\cdot 10^{-6}\ \mathrm{K}^{-1}]. \tag{62}$$

In order to compute an upper bound for the potential effect of anomalous thermal expansion of pore water on the hygrothermic coefficient, the largest value is taken from Eq. (62), $\alpha_{H_2O}^{conf} = 212.10\cdot 10^{-6}\ \mathrm{K}^{-1}$, and assigned to the entire pore water, irrespective of the pore size. Corresponding hygrothermic coefficients are calculated by analogy to the procedure described above for the regular bulk thermal expansion of pore water. The results underline that consideration of anomalous thermal expansion of confined pore water indeed yields larger

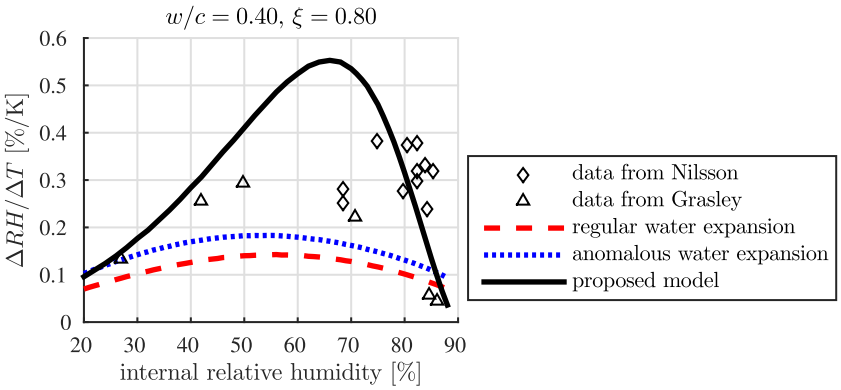

Fig. 11. Hygrothermic coefficients resulting from regular and anomalous thermal expansion of liquid pore water, and comparison with experimentally measured values by Nilsson [17] and Grasley [10]; for mature cement pastes with initial water-to-cement mass ratio w/c = 0.40 and hydration degree ξ = 0.80.

hygrothermic coefficients than the consideration of the thermal expansion of regular bulk pore water, as can be seen from the dashed and dotted graphs in Fig. 11. However, consideration of anomalous thermal expansion of confined pore water alone still cannot explain the experimentally measured hygrothermic coefficients. This implies the existence of another phenomenon, governing the hygrothermic deformations in cement paste, such as the water uptake/release of hydrates, investigated in the present contribution.

4.4. Future outlook

As regards quantification of phase volume fractions, the present study is based on Powers' hydration model. The latter was developed based on water vapor sorption experiments and on the assumption that the mass density of hydrates is constant. The model suggests that gel/capillary porosities are decreasing/increasing *linearly* with increasing hydration degree.

Powers' model was challenged by nuclear magnetic resonance (NMR) measurements documented by Muller et al. [77,78]. They quantified the amounts of water in different confinement states. Weakly and strongly confined *liquid* water was associated with capillary pores and gel pores, respectively. A corresponding hydration model was developed, considering that densification of hydrates is governed by restrictions regarding the available precipitation space [79]. The NMR-based model suggests that gel/capillary porosities are decreasing/increasing *nonlinearly* with increasing hydration degree.

It will be interesting to apply the NMR-based hydration model to micromechanics-based modeling of hydrating cement pastes. This, however, is beyond the scope of the present contribution.

5. Conclusions

Results from the presented inverse multiscale analysis of mature cement pastes suggest that temperature changes are likely to result in a quasi-instantaneous water uptake/release by hydration products. This is an effect for which no physical measurements were available at the time of submitting the present manuscript. However, such measurements were reported shortly thereafter [27]. This leads to the following conclusions:

- Hydration products appear to release liquid water upon heating, and to take up liquid water upon cooling, already within the room temperature regime. This water uptake/release is likely to result (i) in redistribution of water within nanoscopic pores of partially saturated cementitious materials, as studied herein, and (ii) in pressure changes of pore water of liquid saturated cementitious materials.
- The water uptake/release by hydration products was identified as a function of internal relative humidity, prevailing in air-filled pores just before the temperature change (Fig. 2). Notably, this function is independent of the initial water-to-cement mass ratio and, therefore, a mixture-independent material property of the hydration products.
- The water uptake/release by hydration products is much faster than the transport-related water exchange between a tested specimen and its ambient environment. Therefore, mass conservation of solid and liquid water inside a tested specimen allows for linking the water uptake/release by hydration products to hygrothermic coefficients. The latter are the larger, the smaller the overall porosity, i.e. the smaller the initial water-to-cement mass ratio of mature cement pastes.
- Combining model-predicted hygrothermic coefficients with a three-scale representation of mature cement pastes allows for explaining mixture-independent macroscopic thermal expansion coefficients of mature cement pastes as a function of relative humidity.

Acknowledgments

Financial support by the Austrian Science Fund (FWF), provided within project P 281 31-N32 “Bridging the Gap by Means of Multiscale Structural Analyses”, and interesting discussions with Mr. Nabor Jimenez Segura (TU Wien) are gratefully acknowledged. The first author also gratefully acknowledges financial support by the China Scholarship Council (CSC).

Appendix A. Bertherlot's equation

The free energies of cohesion of a pair of solid particles, W^{ss}, and of a pair of liquid particles, $W^{\ell\ell}$, are defined as

$$W^{ss} = 2\,\gamma^{sg}, \quad W^{\ell\ell} = 2\,\gamma^{\ell g}, \tag{A.1}$$

where γ^{sg} and $\gamma^{\ell g}$ are surface tensions between solid and gas and between liquid and gas, respectively. Thermodynamically, the free energy of adhesion of a pair of one solid and one liquid particle, $W^{s\ell}$, equals the work, required to separate the two particles [51,52], i.e.

$$W^{s\ell} = \gamma^{\ell g} + \gamma^{sg} - \gamma^{s\ell}. \tag{A.2}$$

Berthelot's averaging rule [50] approximates the free energy of adhesion $W^{s\ell}$ as the geometric mean of the free energies of cohesion of solid pair and of liquid pair, i.e.

$$W^{s\ell} \approx \sqrt{W^{\ell\ell}\, W^{ss}}. \tag{A.3}$$

Eq. (A.3) was originally proposed by Berthelot for the quantification of particle interactions in mixtures of two gases, based on knowledge regarding particle interactions in the pure gas phases [50]. Inserting Eq. (A.1) into Eq. (A.3) gives

$$W^{s\ell} = 2\sqrt{\gamma^{\ell g}\, \gamma^{sg}}. \tag{A.4}$$

Combining Eqs. (A.2) and (A.4) delivers Berthelot's state equation, see Eq. (18). Notably, Berthelot's approximation, i.e. Eq. (A.3), is reliable only if $W^{\ell\ell} \approx W^{ss}$, i.e. if $\gamma^{\ell g} \approx \gamma^{sg}$ [51], and, hence, if $\theta \approx 0$ such that $\cos\theta \approx 1$. This is the case for cementitious materials.

Appendix B. Proof of Eq. (50)

The aim of this Appendix is to prove that the homogenized thermal expansion coefficient of cement paste is equal to that of the hydrates and clinker, provided that (i) the latter two are equal, i.e. $\alpha_{hyd} = \alpha_{clin}$, and (ii) that pore pressures remain unchanged.

Considering a matrix-inclusion composite with two solid phases, the eigenstresses of the two solids are related to equivalent eigenstrains as

$$\boldsymbol{\sigma}_k^E = -\mathbb{C}_k : \alpha_k \Delta T \boldsymbol{1}, \quad k \in [m; i]. \tag{B.1}$$

In Eq. (B.1), it was considered that the matrix and the inclusion phase exhibit *the same* coefficient of thermal expansion, α_{sol}. Inserting Eq. (B.1) into Eq. (36) and considering that the strain concentration tensors are isotropic,

$$\boldsymbol{\Sigma}_{\text{hom}}^E = -[f_m \mathbb{C}_m : \mathbb{A}_m + f_i \mathbb{C}_i : \mathbb{A}_i] : \alpha_{sol} \Delta T \boldsymbol{1}. \tag{B.2}$$

Relating the macroscopic (i.e. "homogenized") eigenstrains to equivalent eigenstresses by analogy to Eq. (B.1), inserting Eq. (B.2) into the resulting expression, and considering Eq. (35) gives

$$\mathbf{E}_{\text{hom}}^E = -\mathbb{C}_{\text{hom}}^{-1} : \boldsymbol{\Sigma}_{\text{hom}}^E = \alpha_{sol} \Delta T \boldsymbol{1}. \tag{B.3}$$

Finally, consideration of the definition of the homogenized coefficient of thermal expansion according to

$$\mathbf{E}_{\text{hom}}^E = \alpha_{\text{hom}} \Delta T \boldsymbol{1}, \tag{B.4}$$

and comparison of Eqs. (B.3) and (B.4) completes the desired proof

$$\alpha_{\text{hom}} = \alpha_{sol}. \tag{B.5}$$

Considering a matrix-inclusion composite with a solid matrix and pores, whereby the latter do not exhibit a pore pressure change, the change of homogenized eigenstresses, resulting from a temperature change, reads, analogous to Eq. (B.2), as

$$\boldsymbol{\Sigma}_{\text{hom}}^E = -f_m \mathbb{C}_m : \mathbb{A}_m : \alpha_{sol} \Delta T \boldsymbol{1}. \tag{B.6}$$

The homogenized stiffness reads as

$$\mathbb{C}_{\text{hom}} = f_m \mathbb{C}_m : \mathbb{A}_m. \tag{B.7}$$

Therefore, Eq. (B.3) also holds for Eqs. (B.6) and (B.7). A comparison of Eqs. (B.3) and (B.4) completes the proof also for porous two-phase materials, see Eq. (B.5).

Appendix C. Refined analysis concerning thermal expansion of cement clinker and hydrates

In Section 2.6, the thermal expansion of cement clinker was assumed, in the sense of a reductionist approach, to be equal to that of the hydrates. In the following, this assumption is assessed from the viewpoint of a more refined analysis.

The thermal expansion coefficient of tricalcium silicate (C_3S) amounts to [80]

$$\alpha_{C_3S} = 13.5 \cdot 10^{-6}\ \text{K}^{-1}. \tag{C.1}$$

Given that 45–75% of typical Portland cements consist of C_3S provides the motivation to set the thermal expansion coefficient of cement clinker, α_{clin}, equal to α_{C_3S} according to Eq. (C.1). This allows, in combination with the thermal expansion coefficient of fully dried mature cement pastes, $\alpha_{cp}(RH = 0\%) = 12.5 \cdot 10^{-6}\,\text{K}^{-1}$, see Fig. 1, for identifying the thermal expansion coefficient of hydrates, based on the presented multiscale model. The identification follows the steps listed in Table 3, whereby all the pore pressures are set equal to zero, because $RH = 0\%$. The identification is carried out for values of the initial water-to-cement mass ratio amounting to 0.40, 0.50, 0.60, and 0.70. The identified thermal expansion coefficients of hydrates differ in the fourth significant digit (Table C.4). In addition, the thermal expansion coefficients of the cement clinker, $\alpha_{clin} \approx 13.5 \cdot 10^{-6}\,\text{K}^{-1}$, and of the hydrates, $\alpha_{hyd} \approx 12.4 \cdot 10^{-6}\,\text{K}^{-1}$, do not differ significantly from that of fully dried mature cement pastes, $\alpha_{cp}(RH = 0\%) = 12.5 \cdot 10^{-6}\,\text{K}^{-1}$. This justifies the simplifying assumption of $\alpha_{cp}(RH = 0\%) = \alpha_{hyd} = \alpha_{clin} = 12.5 \cdot 10^{-6}\,\text{K}^{-1}$, see Eq. (50).

Table C.4
w/c-dependent thermal expansion coefficients of solid hydrates, identified by means of the presented multiscale model (see Table 3) from the thermal expansion coefficients of unhydrated clinker, $\alpha_{clin} = 13.5 \cdot 10^{-6}\,\text{K}^{-1}$, and of fully dried mature cement paste, $\alpha_{cp}(RH = 0\%) = 12.5 \cdot 10^{-6}\,\text{K}^{-1}$.

w/c [−]	0.40	0.50	0.60	0.70
α_{hyd} [$10^{-6}\,\text{K}^{-1}$]	12.33	12.35	12.37	12.38

Appendix D. Regression functions, reproducing model-predicted hygrothermic coefficients

In order to render the model-predicted hygrothermic coefficients shown in Fig. 8 accessible, the following regression polynomial is introduced:

$$\Delta RH/\Delta T = \sum_{i=0}^{6} a_i \, RH^i. \tag{D.1}$$

The coefficients a_i (i = 0,…,6) depend on the initial water-to-cement mass ratio, as expressed by the following polynomials

$$a_i = \sum_{j=0}^{3} k_j^i (w/c)^j, \tag{D.2}$$

with optimal coefficients k_j^i listed in Table D1.

Table D1
Coefficients of polynomial fitting function in Eq. (D.2).

i	0	1	2	3	4	5	6
k_0^i	0.005355	−0.05546	0.2130	0.005258	−0.9653	1.8967	−1.1860
k_1^i	0.08929	−1.4833	9.8072	−33.5640	60.8282	−56.9151	21.6848
k_2^i	−0.2411	3.8638	−24.7217	81.2707	−142.5594	128.5975	−46.9403
k_3^i	0.1628	−2.5807	16.3225	−52.8942	91.6319	−81.4640	29.2167

References

[1] R. Helmuth, Dimensional changes of hardened Portland cement pastes caused by temperature changes, Highway Research Board Proceedings, vol. 40, 1961, pp. 315–335.
[2] Z. Bažant, Delayed thermal dilatations of cement paste and concrete due to mass transport, Nucl. Eng. Des. 14 (2) (1970) 308–318.
[3] E. Sellevold, Ø. Bjøntegaard, Coefficient of thermal expansion of cement paste and concrete: mechanisms of moisture interaction, Mater. Struct. 39 (9) (2006) 809–815.
[4] H. Ai, J.F. Young, G.W. Scherer, Thermal expansion kinetics: method to measure permeability of cementitious materials, II. Application to hardened cement pastes, J. Am. Ceram. Soc. 84 (2) (2001) 385–391.
[5] J. Ciardullo, D. Sweeney, G. Scherer, Thermal expansion kinetics: method to measure permeability of cementitious materials, IV. Effect of thermal gradients and viscoelasticity, J. Am. Ceram. Soc. 88 (5) (2005) 1213–1221.
[6] S. Meyers, Thermal expansion characteristics of hardened cement paste and of concrete, Highway Research Board Proceedings, vol. 30, 1951, pp. 193–203.
[7] L.J. Mitchell, Thermal Expansion Tests on Aggregates, Neat Cements, and Concretes, Proceedings of the American Society for Testing and Materials, vol. 53, 1953, pp. 963–977.
[8] H. Dettling, Die Wärmedehnung des Zementsteines, der Gesteine und der Betone [Thermal Expansion of Cement Pastes, Aggregates, and Concretes], Technische Hochschule Stuttgart, 1962 Dr.-Ing. thesis.
[9] J.H. Emanuel, J.L. Hulsey, Prediction of the thermal coefficient of expansion of concrete, J. Am. Concr. Inst. 74 (4) (1977) 149–155.
[10] Z.C. Grasley, D.A. Lange, Thermal dilation and internal relative humidity of hardened cement paste, Mater. Struct. 40 (3) (2007) 311–317.
[11] H. Wang, E. Binder, H. Mang, Y. Yuan, B. Pichler, Multiscale structural analysis inspired by exceptional load cases concerning the immersed tunnel of the Hong Kong-Zhuhai-Macao Bridge, Undergr. Space (2018), http://dx.doi.org/10.1016/j.undsp.2018.02.001.
[12] K. Sakyi-Bekoe, Assessment of the Coefficient of Thermal Expansion of Alabama Concrete, Auburn University, Alabama, 2008 Master thesis.
[13] A.K. Mukhopadhyay, S. Neekhra, D.G. Zollinger, Preliminary characterization of aggregate coefficient of thermal expansion and gradation for paving concrete, Tech. Rep. 0-1700-5, Texas Transportation Institute, 2007.
[14] G.A. Khoury, B.N. Grainger, P.J. Sullivan, Transient thermal strain of concrete: literature review, conditions within specimen and behaviour of individual constituents, Mag. Concr. Res. 37 (132) (1985) 131–144.
[15] Z.P. Bažant, M.F. Kaplan, Concrete at High Temperatures: Material Properties and Mathematical Models, Longman, Burnt Mill, England, 1996.
[16] Y.-F. Fu, Y.-L. Wong, C.-S. Poon, C.-A. Tang, P. Lin, Experimental study of micro/macro crack development and stress-strain relations of cement-based composite materials at elevated temperatures, Cem. Concr. Res. 34 (5) (2004) 789–797.
[17] L.-O. Nilsson, Temperature effects in relative humidity measurements on concrete — some preliminary studies, Symposium and Day of Building Physics, Swedish Council for Building Research, Lund, Sweden, 1987, pp. 456–462.
[18] B. Persson, Self-desiccation and chloride migration, Proceedings of 3rd International Research Seminar, Lund Institute of Technology, Lund, Sweden, 2002, pp. 175–194.
[19] F. Radjy, E.J. Sellevold, K.K. Hansen, Isoteric vapor pressure: temperature data for water sorption in hardened cement paste: enthalpy, entropy and sorption isotherms at different temperatures, Tech. Rep. BYG-DTUR-057, Technical University of Denmark, 2003.
[20] N. Vargaftik, B. Volkov, L. Voljak, International tables of the surface tension of water, J. Phys. Chem. Ref. Data 12 (3) (1983) 817–820.
[21] M. Wyrzykowski, P. Lura, Moisture dependence of thermal expansion in cement-based materials at early ages, Cem. Concr. Res. 53 (2013) 25–35.
[22] P. Lura, O.M. Jensen, K. van Breugel, Autogenous shrinkage in high-performance cement paste: an evaluation of basic mechanisms, Cem. Concr. Res. 33 (2) (2003) 223–232.
[23] I. Vlahinić, H.M. Jennings, J.J. Thomas, A constitutive model for drying of a partially saturated porous material, Mech. Mater. 41 (3) (2009) 319–328.
[24] D.P. Bentz, E.J. Garboczi, D.A. Quenard, Modelling drying shrinkage in reconstructed porous materials: application to porous Vycor glass, Model. Simul. Mater. Sci. Eng. 6 (3) (1998) 211.
[25] S. Mindess, J.F. Young, D. Darwin, Concrete, Prentice Hall, 2003.
[26] L. Dormieux, D. Kondo, F.-J. Ulm, Microporomechanics, John Wiley & Sons, 2006.
[27] M. Wyrzykowski, P.J. McDonald, K.L. Scrivener, P. Lura, Water redistribution within the microstructure of cementitious materials due to temperature changes studied with ^{1}H NMR, J. Phys. Chem. C 121 (50) (2017) 27950–27962.
[28] A.J. Allen, J.J. Thomas, H.M. Jennings, Composition and density of nanoscale calcium-silicate-hydrate in cement, Nat. Mater. 6 (4) (2007) 311–316.
[29] H.M. Jennings, Refinements to colloid model of C-S-H in cement: CM-II, Cem. Concr. Res. 38 (3) (2008) 275–289.
[30] R. Badmann, N. Stockhausen, M.J. Setzer, The statistical thickness and the chemical potential of adsorbed water films, J. Colloid Interface Sci. 82 (2) (1981) 534–542.
[31] Q. Huang, Z. Jiang, X. Gu, W. Zhang, B. Guo, Numerical simulation of moisture transport in concrete based on a pore size distribution model, Cem. Concr. Res. 67 (2015) 31–43.
[32] S. Brunauer, J. Skalny, E. Bodor, Adsorption on nonporous solids, J. Colloid Interface Sci. 30 (4) (1969) 546–552.
[33] Y. Xi, Z.P. Bažant, H.M. Jennings, Moisture diffusion in cementitious materials: adsorption isotherms, Adv. Cem. Based Mater. 1 (6) (1994) 248–257.
[34] B. Pichler, L. Dormieux, Cracking risk of partially saturated porous media — part I: microporoelasticity model, Int. J. Numer. Anal. Methods Geomech. 34 (2) (2010) 135–157.
[35] B. Pichler, L. Dormieux, Cracking risk of partially saturated porous media — Part II: application to drying shrinkage, Int. J. Numer. Anal. Methods Geomech. 34 (2) (2010) 159–186.
[36] T. Mori, K. Tanaka, Average stress in matrix and average elastic energy of materials with misfitting inclusions, Acta Metall. 21 (5) (1973) 571–574.
[37] Y. Benveniste, A new approach to the application of Mori-Tanaka's theory in composite materials, Mech. Mater. 6 (2) (1987) 147–157.
[38] B. Pichler, C. Hellmich, J. Eberhardsteiner, Spherical and acicular representation of hydrates in a micromechanical model for cement paste: prediction of early-age elasticity and strength, Acta Mech. 203 (3–4) (2009) 137–162.
[39] B. Pichler, C. Hellmich, Upscaling quasi-brittle strength of cement paste and mortar: a multi-scale engineering mechanics model, Cem. Concr. Res. 41 (5) (2011) 467–476.
[40] F.-J. Ulm, G. Constantinides, F. Heukamp, Is concrete a poromechanics materials? — a multiscale investigation of poroelastic properties, Mater. Struct. 37 (1) (2004) 43–58.

[41] T.C. Powers, T.L. Brownyard, Studies of the physical properties of hardened Portland cement paste, J. Am. Concr. Inst. 18 (1946) 101–132.
[42] T.C. Powers, Structure and physical properties of hardened Portland cement paste, J. Am. Ceram. Soc. 41 (1) (1958) 1–6.
[43] T.C. Hansen, Physical structure of hardened cement paste. A classical approach, Mater. Struct. 19 (6) (1986) 423–436.
[44] P. Acker, Micromechanical Analysis of Creep and Shrinkage Mechanisms, Creep, Shrinkage and Durability Mechanics of Concrete and Other Quasi-brittle Materials, Cambridge, MA, (2001), pp. 15–25.
[45] A.V. Neimark, P.I. Ravikovitch, Capillary condensation in MMS and pore structure characterization, Microporous Mesoporous Mater. 44 (2001) 697–707.
[46] M. Tanaka, G. Girard, R. Davis, A. Peuto, N. Bignell, Recommended table for the density of water between 0 °C and 40 °C based on recent experimental reports, Metrologia 38 (4) (2001) 301.
[47] C. Hua, P. Acker, A. Ehrlacher, Analyses and models of the autogenous shrinkage of hardening cement paste: I. Modelling at macroscopic scale, Cem. Concr. Res. 25 (7) (1995) 1457–1468.
[48] H. Chen, M. Wyrzykowski, K. Scrivener, P. Lura, Prediction of self-desiccation in low water-to-cement ratio pastes based on pore structure evolution, Cem. Concr. Res. 49 (2013) 38–47.
[49] A. Wongkoblap, D. Do, G. Birkett, D. Nicholson, A critical assessment of capillary condensation and evaporation equations: a computer simulation study, J. Colloid Interface Sci. 356 (2) (2011) 672–680.
[50] D. Berthelot, Sur le mélange des gaz [Mixtures of gases], Compt. Rendus 126 (1898) 1703–1706.
[51] D.Y. Kwok, A.W. Neumann, Contact angle measurement and contact angle interpretation, Adv. Colloid Interf. Sci. 81 (3) (1999) 167–249.
[52] D. Li, A. Neumann, Equation of state for interfacial tensions of solid-liquid systems, Adv. Colloid Interf. Sci. 39 (1992) 299–345.
[53] K. Maekawa, T. Ishida, T. Kishi, Multi-scale Modeling of Structural Concrete, CRC Press, 2008.
[54] V. Baroghel-Bouny, Water vapour sorption experiments on hardened cementitious materials: part I: essential tool for analysis of hygral behaviour and its relation to pore structure, Cem. Concr. Res. 37 (3) (2007) 414–437.
[55] V. Baroghel-Bouny, T. Chaussadent, Texture and moisture characterization of hardened cement pastes and concretes from water vapour sorption measurements, in: H. Jennings, K. Scrivener, J. Kropp (Eds.), The modelling of microstructure and its potential for studying transport properties and durability, Nato ASI Series, vol. 304, Kluwer Academic Publishers, Boston, 1996, pp. 241–255.
[56] M.B. Pinson, E. Masoero, P.A. Bonnaud, H. Manzano, Q. Ji, S. Yip, J.J. Thomas, M.Z. Bažant, K.J. Van Vliet, H.M. Jennings, Hysteresis from multiscale porosity: modeling water sorption and shrinkage in cement paste, Phys. Rev. Appl. 3 (6) (2015) 064009.
[57] S. Brunauer, P.H. Emmett, E. Teller, Adsorption of gases in multimolecular layers, J. Am. Chem. Soc. 60 (2) (1938) 309–319.
[58] M. Irfan-ul Hassan, B. Pichler, R. Reihsner, C. Hellmich, Elastic and creep properties of young cement paste, as determined from hourly repeated minute-long quasi-static tests, Cem. Concr. Res. 82 (2016) 36–49.
[59] A. Zaoui, Continuum micromechanics: survey, J. Eng. Mech. 128 (8) (2002) 808–816.
[60] B. Pichler, C. Hellmich, Estimation of influence tensors for eigenstressed multiphase elastic media with nonaligned inclusion phases of arbitrary ellipsoidal shape, J. Eng. Mech. 136 (8) (2010) 1043–1053.
[61] V. Levin, Coefficients of temperature expansion of heterogeneous materials, Mech. Solids 2 (1967) 88–94.
[62] J.D. Eshelby, The determination of the elastic field of an ellipsoidal inclusion, and related problems, Proc. R. Soc. London, Ser. A 241 (1226) (1957) 376–396.
[63] T.C. Powers, The thermodynamics of volume change and creep, Mater. Struct. 1 (6) (1968) 487–507.
[64] Z. Bažant, Thermodynamics of interacting continua with surfaces and creep analysis of concrete structures, Nucl. Eng. Des. 20 (2) (1972) 477–505.
[65] Z. Bažant, J. Chern, Concrete creep at variable humidity: constitutive law and mechanism, Mater. Struct. 18 (1) (1985) 1.
[66] Z.P. Bažant, A.B. Hauggaard, S. Baweja, F.-J. Ulm, Microprestress-solidification theory for concrete creep. I: aging and drying effects, J. Eng. Mech. 123 (11) (1997) 1188–1194.
[67] M. Wyrzykowski, P. Lura, The effect of external load on internal relative humidity in concrete, Cem. Concr. Res. 65 (2014) 58–63.
[68] J.J. Valenza, G.W. Scherer, Evidence of anomalous thermal expansion of water in cement paste, Cem. Concr. Res. 35 (1) (2005) 57–66.
[69] S. Ghabezloo, J. Sulem, J. Saint-Marc, The effect of undrained heating on a fluid-saturated hardened cement paste, Cem. Concr. Res. 39 (1) (2009) 54–64.
[70] S. Ghabezloo, Micromechanics analysis of thermal expansion and thermal pressurization of a hardened cement paste, Cem. Concr. Res. 41 (5) (2011) 520–532.
[71] L. Parrott, Basic creep, drying creep and shrinkage of a mature cement paste after a heat cycle, Cem. Concr. Res. 7 (5) (1977) 597–604.
[72] X. Cong, R.J. Kirkpatrick, Effects of the temperature and relative humidity on the structure of C-S-H gel, Cem. Concr. Res. 25 (6) (1995) 1237–1245.
[73] J.J. Thomas, H.M. Jennings, Effect of heat treatment on the pore structure and drying shrinkage behavior of hydrated cement paste, J. Am. Ceram. Soc. 85 (9) (2002) 2293–2298.
[74] A. Gajewicz, E. Gartner, K. Kang, P. McDonald, V. Yermakou, A ^{1}H NMR relaxometry investigation of gel-pore drying shrinkage in cement pastes, Cem. Concr. Res. 86 (2016) 12–19.
[75] H.M. Jennings, A. Kumar, G. Sant, Quantitative discrimination of the nano-pore-structure of cement paste during drying: new insights from water sorption isotherms, Cem. Concr. Res. 76 (2015) 27–36.
[76] S. Xu, G.W. Scherer, T. Mahadevan, S.H. Garofalini, Thermal expansion of confined water, Langmuir 25 (9) (2009) 5076–5083.
[77] A. Muller, K. Scrivener, A. Gajewicz, P. McDonald, Densification of C-S-H measured by ^{1}H NMR relaxometry, J. Phys. Chem. C 117 (1) (2012) 403–412.
[78] A. Muller, K. Scrivener, A. Gajewicz, P. McDonald, Use of bench-top NMR to measure the density, composition and desorption isotherm of C-S-H in cement paste, Microporous Mesoporous Mater. 178 (2013) 99–103.
[79] M. Königsberger, C. Hellmich, B. Pichler, Densification of C-S-H is mainly driven by available precipitation space, as quantified through an analytical cement hydration model based on NMR data, Cem. Concr. Res. 88 (2016) 170–183.
[80] J. Piasta, Heat deformations of cement paste phases and the microstructure of cement paste, Mater. Struct. 17 (6) (1984) 415–420.
[81] L. Dormieux, A. Molinari, D. Kondo, Micromechanical approach to the behavior of poroelastic materials, J. Mech. Phys. Solids 50 (10) (2002) 2203–2231.